The Astrophysical Journal Letters, 837:L12 (5pp), 2017 March 1 https://doi.org/10.3847/2041-8213/aa5ff7

High Lyman Continuum Escape Fraction in a Lensed Young Compact Dwarf Galaxy at $z = 2.5$

Fuyan Bian[1,5], Xiaohui Fan[2], Ian McGreer[2], Zheng Cai[3,6], and Linhua Jiang[4]
[1] Research School of Astronomy & Astrophysics, Mt Stromlo Observatory, Australian National University, Canberra, ACT 2611, Australia
[2] Steward Observatory, University of Arizona, 933 N Cherry Avenue, Tucson, AZ 85721, USA
[3] UCO/Lick Observatory, University of California, 1156 High Street, Santa Cruz, CA 95064, USA
[4] Kavli Institute for Astronomy and Astrophysics, Peking University, Beijing 100871, China
Received 2017 January 16; revised 2017 February 9; accepted 2017 February 10; published 2017 March 2

Abstract

We present the *HST* WFC3/F275W UV imaging observations of A2218-Flanking, a lensed compact dwarf galaxy at redshift $z \approx 2.5$. The stellar mass of A2218-Flanking is $\log(M_*/M_\odot) = 9.14^{+0.07}_{-0.04}$ and SFR is $12.5^{+3.8}_{-7.4}\ M_\odot\ \mathrm{yr}^{-1}$ after correcting the magnification. This galaxy has a young galaxy age of 127 Myr and a compact galaxy size of $r_{1/2} = 2.4$ kpc. The *HST* UV imaging observations cover the rest-frame Lyman continuum (LyC) emission (∼800 Å) from A2218-Flanking. We firmly detect (14σ) the LyC emission in A2218-Flanking in the F275W image. Together with the *HST* F606W images, we find that the absolute escape fraction of LyC is $f_{\mathrm{abs,esc}} > 28\%$–$57\%$ based on the flux density ratio between 1700 and 800 Å (f_{1700}/f_{800}). The morphology of the LyC emission in the F275W images is extended and follows the morphology of the UV continuum morphology in the F606W images, suggesting that the f_{800} is not from foreground contaminants. We find that the region with a high star formation rate surface density has a lower f_{1700}/f_{800} (higher f_{800}/f_{1700}) ratio than the diffused regions, suggesting that LyC photons are more likely to escape from the region with the intensive star-forming process. We compare the properties of galaxies with and without LyC detections and find that LyC photons are easier to escape in low-mass galaxies.

Key words: cosmology: observations – dark ages, reionization, first stars – galaxies: high-redshift – gravitational lensing: strong

1. Introduction

Observations of high-redshift quasars and galaxies and the cosmic microwave background have revealed the reionization history of the universe, which occurred at a redshift of $z = 8$–9 and largely finished at $z = 6$ (e.g., Fan et al. 2006a, 2006b; Stark et al. 2011; Robertson et al. 2013; Schenker et al. 2014; Bian et al. 2015; Bouwens et al. 2015a; Planck Collaboration et al. 2016). Ionizing photons emitted from high-redshift galaxies are widely considered the major sources to reionize the universe. There are three key parameters regulating the reionization process: the total produced Lyman continuum (LyC) ionizing photons, the LyC photon escape fraction (f_{esc}), and the intergalactic medium (IGM) clumping factor (e.g., Robertson et al. 2013). The IGM clumping factor is difficult to measure using observations, but it can be estimated by simulations (e.g., Pawlik et al. 2009). The total ionizing photons produced by high-redshift galaxies can be constrained by the luminosity function and LyC photon production efficiency of high-redshift galaxies (e.g., Bouwens et al. 2015b, 2016; Livermore et al. 2017). To contribute enough ionizing photons to reionize the universe, it is required that the LyC escape fraction (f_{esc}) be comparable to or larger than $f_{\mathrm{esc}} = 0.2$ at the epoch of the reionization (e.g., Ouchi et al. 2009; Robertson et al. 2013). However, the fraction of the total LyC photons that can escape from galaxies has not been well measured.

Due to the large optical depth of IGM, it is very difficult to measure the LyC escape fraction in galaxies at $z > 4$. Extensive observations have been carried out to search for LyC leaking in nearby galaxies using far-ultraviolet spectroscopy (e.g., Leitet et al. 2013; Izotov et al. 2016a, 2016b; Leitherer et al. 2016), and to search for high-redshift galaxies at $z = 1$–4 using deep blue optical spectroscopy (e.g., Steidel et al. 2001; Shapley et al. 2006, 2016; Nestor et al. 2013) and/or narrow/intermediate/broadband UV imaging (e.g., Siana et al. 2007, 2015; Vanzella et al. 2010; Nestor et al. 2011; Cooke et al. 2014; Naidu et al. 2016; Rutkowski et al. 2016; Vasei et al. 2016). However, accurately measuring the escape fraction remains difficult. Most of the studies on the escape fraction in high-redshift star-forming galaxies have null detection and can only obtain upper limits ($f_{\mathrm{esc}} < 2\%$–20%), even with deep stacked UV images. Meanwhile, the escape fraction in high-redshift galaxies may be overestimated, due to foreground contamination, especially for results based on ground-based, seeing-limited observations (e.g., Vanzella et al. 2012). Therefore, it is crucial to carry out deep, high spatial resolution imaging follow-up observations to rule out potential foreground interlopers. To date, there are only a few convincing detections of LyC emission in galaxies at $z \sim 3$, including *ion*2 (Vanzella et al. 2016) and Q1549-C25 (Shapley et al. 2016).

To address the above problems, we study the LyC escape fraction in a sample of gravitationally lensed galaxies at $z \sim 2$–3 using *HST* WFC3 UV imaging observations. The high-spatial-resolution *HST* images rule out foreground contamination and put strong constraints on the LyC escape fraction in these lensed galaxies. In this Letter, we report a high LyC escape fraction in one of the galaxies in our *HST* program, a lensed compact dwarf galaxy, A2218-Flanking, at $z = 2.518$. Throughout this paper, the following cosmological parameters

[5] Stromlo Fellow.
[6] Hubble Fellow.

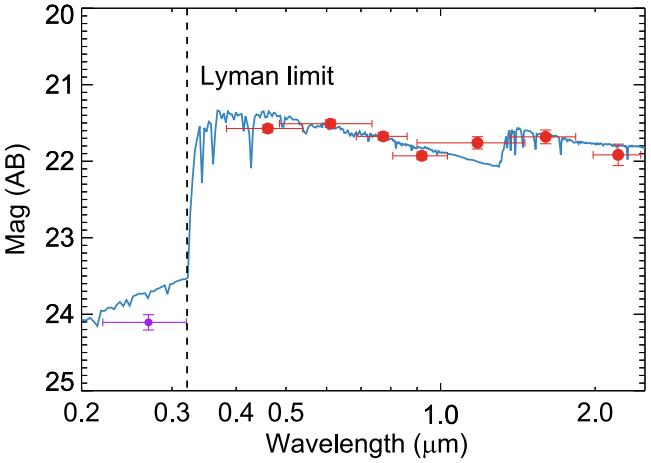

Figure 1. Spectral energy distribution (SED) fitting result of A2218-Flanking. The blue curve represents the best-fit stellar synthesis model with a constant star formation history. We do not apply the interstellar medium and IGM extinction correction for the blue curve. The red points are the dereddened photometry data based on the $E(B-V)=0.11$, which is derived from the SED fitting. The purple data point represents the photometry data from *HST* WFC3/F275W band, which covers the blueward Lyman limits of A2218-Flanking. The data point has been corrected for IGM attenuation with $\exp(-\tau_{\rm IGM,800})=0.73$ (see Section 3.2 for more detail). The dashed line represents the Lyman limit at $z=2.518$.

are used: Hubble constant $H_0=70\ {\rm km\ s^{-1}\ Mpc^{-1}}$, dark matter density $\Omega_{\rm M}=0.30$, and dark energy density $\Omega_\Lambda=0.70$ for a flat universe. The distance is given in physical distance. All the magnitudes are expressed in the AB magnitude system.

2. Observations and Data Reduction

A2218-Flanking is a compact dwarf galaxy at the redshift of $z=2.518$, which is lensed by the Abell 2218 galaxy cluster (Richard et al. 2011). Here we summarize the properties of A2218-Flanking based on the Keck/NIRSPEC near-IR spectroscopic and *HST* imaging observations (Richard et al. 2011). A2218-Flanking consists of two components. The total magnification factor for the two components is 13 ± 2.5. The size of A2218-Flanking is compact, with a half-light radius of $r_{1/2}=2.36\pm0.55$ kpc on the source plane. The gas-phase oxygen abundance in A2218-Flanking is less than 20% of the solar abundance ($12+\log({\rm O/H})<8.05$), based on the N2 metallicity indicator (Pettini & Pagel 2004). We refer the readers to Richard et al. (2011) for more detail.

We carry out UV imaging observations of A2218-Flanking using the *HST*/WFC3 UVIS channel in the F275W band to cover the LyC emission (Figure 1). The F275W band covers the observed-frame wavelength from 2200 to 3200 Å, which corresponds to the rest-frame wavelength of 625–910 Å at $z=2.518$ to ensure that there are no photons redward of LyC (912 Å) to contaminate the LyC measurements. This observation is part of *HST* proposal program 3349 (PI: X. Fan). In this program, we study the LyC escape fraction in seven lensed star-forming galaxies at $z=2.0$–2.5, including A2218-Flanking, A2218-Ebbels, CLONE, MACS0451, J0900+2234, J0901+1814, and J1343+4155. A2218-Flanking is the only galaxy detected in the LyC images. A total of three orbits (9538 s) of exposure on A2218-Flanking are obtained. The observations contain a six-point dithering sequence. To solve the WFC3/UVIS low charge transfer efficiency issue, we apply a background of $12e^-$/pixel to each image to preserve faint signals and place A2218-Flanking at the bottom-left corner of WFC3/UVIS chip2, which is close to the WFC3/UVIS detector amplifier.

We use the *HST* WPFC2/F606W (ID: 7343, PI: Gordon Squires) image as the reference image to determine the position and detection region for A2218-Flanking. We use bright stars to align the F275 image to the F606W image, after reducing the individual F275 imaging data with the standard WFC3-UV data reduction pipeline. We combine the individual images in F275W and F606W using `Astrodrizzle` 2.1.3, with a final pixel scale = 0.0396 arcsec/pixel and a final pixfrac = 0.8. Figure 2 shows the A and B components of A2218-Flanking in the F275W and F606W images.

3. Results

3.1. Stellar Population of A2218-Flanking

We use the Hyperz program (Bolzonella et al. 2000) to fit the Bruzual & Charlot (2003) stellar synthesis models to the spectral energy distribution (SED) of A2218-Flanking, including broadband photometry of *HST* F475W (B), F606W (V), F775W (I'), F850LP, F110W (J), F160W (H) bands, and the ground-based K band, which are adopted from Richard et al. (2011). We use the stellar synthesis models with a Salpeter Initial Mass Function (IMF; Salpeter 1955), a 0.2 solar metallicity ($Z=0.004$), and a continuous star formation history with constant SFR. We apply a Small Magellanic Cloud (SMC) dust extinction curve (Prevot et al. 1984) rather than the commonly used Calzetti et al. (2000) dust extinction law, because the latter one results in an unphysically young galaxy star formation age ($t_{\rm SF}<10$ Myr) for A2218-Flanking. Reddy et al. (2010) suggested that the SMC-like extinction curve may better describe this type of galaxies.

Figure 1 shows the SED fitting results. We find that the galaxy age is 127^{+33}_{-14} Myr and the dust extinction is $E(B-V)=0.11$. After corrected for the lensing magnification ($\mu=2.78$ mag), the stellar mass is $\log(M_*/M_\odot)=9.14^{+0.07}_{-0.04}$, which is about an order of magnitude smaller than that in typical star-forming galaxies at $z\sim2-3$, and the SFR is $12.5^{+3.8}_{-7.4}\ M_\odot\ {\rm yr^{-1}}$. The star formation rate (SFR) derived from the SED fitting is consistent with the dust-corrected UV-based SFR, which is $11.0\pm0.1\ M_\odot\ {\rm yr^{-1}}$ but is higher than that in (Richard et al. 2011) by a factor of two. Richard et al. (2011) used the dust-corrected Hα luminosity from slit spectroscopy to estimate the SFR. The Hα-based SFR may be underestimated due to the slit loss and cause this discrepancy. Thus, we adopt the SFR derived from the SED fitting for our further analysis. In the fitting process, we do not take the emission line into account, which results in a slightly larger stellar mass (∼0.1dex) and older galaxy age, but this does not change our main conclusions.

3.2. LyC Escape Fraction

We measure the flux densities of A2218-Flanking in the F275W and F606W images. The F275W band covers the wavelength blueward of LyC at 800 Å, and the F606W band samples the rest-frame UV wavelength at 1700 Å. We use the F606W image as a reference image to define the detection region, in which we will measure the flux in the F275W and F606W images. We consider the pixels with a surface brightness 3σ higher than the background in the F606W image

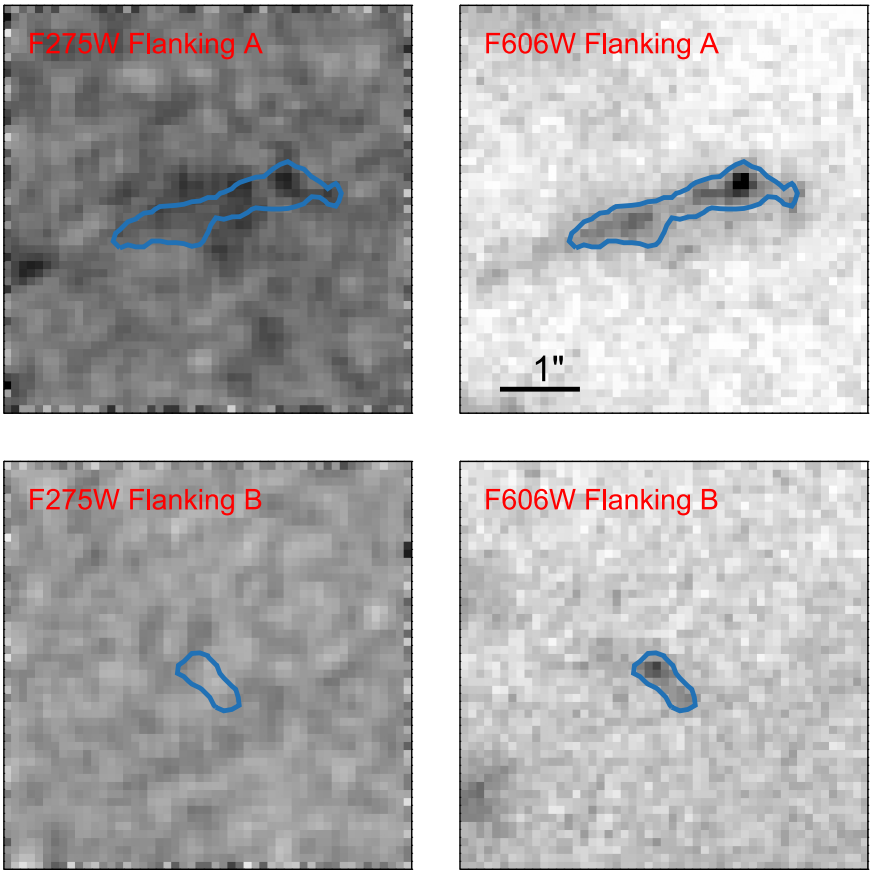

Figure 2. Top panel: F275W (left) and F606W (right) images of the A component of A2218-Flanking. Bottom panel: F275W (left) and F660W (right) images of the B component of A2218-Flanking. The blue contours represent the detection region defined by the surface brightness 3σ above the background in F606W images. North is up, and east is left. For clarity, we smooth the F275W images by 0.″3.

as the detection region. Figure 2 shows the detection regions for the A and B components of A2218-Flanking.

We measure the F275W and F606W fluxes in the detection regions (Figure 2). For the A and B components together, we find a total F275W band flux density of $f_{800} = 0.36 \pm 0.03\,\mu$Jy and a F606W band flux density of $f_{1700} = 1.83 \pm 0.01\,\mu$Jy, which leads to a ratio of $f_{1700}/f_{800} = 4.9 \pm 0.3$. We also measure the flux densities in the A and B components separately. For the A component, we find a F275W band flux density of $f_{800} = 0.36 \pm 0.03\,\mu$Jy and a F606W band flux density of $f_{1700} = 1.67 \pm 0.01\,\mu$Jy, which leads to the ratio $f_{1700}/f_{800} = 4.6 \pm 0.3$. For the B component, we find a F606 band flux density of $f_{1700} = 0.154 \pm 0.002\,\mu$Jy, which is about 10 times fainter than A component. The F275W flux is $f_{800} = -0.006 \pm 0.008$. The 5σ upper limit of the F275W flux for B component is $f_{800} < 0.039\,\mu$Jy. If we assume that the B component holds the same f_{1700}/f_{800} ratio as the A component, the expected F275W flux density of B component will be $f_{800} = 0.033\,\mu$Jy, which is consistent with the fact that the B component is not detected in the F275W image in 5σ. These well-detected LyC fluxes suggest that A2217-Flanking has a high LyC escape fraction.

We estimate the relative LyC escape fraction $f_{\rm esc,rel}$ by the following equation:

$$f_{\rm esc,rel} = \frac{L_{1700}/L_{800}}{f_{1700}/f_{800}} \times \exp(\tau_{\rm IGM,800}), \quad (1)$$

where L_{1700}/L_{800} is the intrinsic luminosity density ratio between 1700 and 800 Å, and f_{1700}/f_{800} is the observed flux density ratio between 1700 and 800 Å. $\tau_{\rm IGM,800}$ is the IGM opacity at 800 Å at $z = 2.5$ (e.g., Madau 1995).

The absolute LyC escape fraction $f_{\rm esc,abs}$ is:

$$f_{\rm esc,abs} = f_{\rm esc,rel} \times 10^{-0.4 \times A_{1700}}, \quad (2)$$

where, A_{1700} represents the dust extinction at 1700 Å.

It is difficult to measure the LyC escape fraction based on one galaxy at $z = 2.5$ accurately due to the uncertainties of the intrinsic luminosity ratio, L_{1700}/L_{800} and IGM opacity, $\tau_{\rm IGM,800}$. First, the intrinsic L_{1700}/L_{800} ratio is very sensitive to galaxy star formation history and galaxy age (Siana et al. 2007). We find the intrinsic $L_{1700}/L_{800} = 6$ based on the galaxy star formation history and galaxy age derived in Section 3.1. To study how the intrinsic L_{1700}/L_{800} ratio changes with star formation history, we also fit the broadband SED with the stellar synthesis models with the exponential declined SFR history (SFR $\propto \exp(t/\tau)$) by changing τ from 0.1 Gyr to 1 Gyr. We find that the exponential declined SFR history usually results in a younger galaxy age (e.g., 91^{+11}_{-38} Myr for $\tau = 0.1$ Gyr), and the intrinsic L_{1700}/L_{800} ratio can be as low as 3.5. Second, It is impossible to determine the IGM opacity for a given random light of sight. We carry out a Monte Carlo (MC) simulation of IGM absorption. We simulate absorption systems in 10,000 lines of sight. These absorption systems follow the distributions of neutral hydrogen column

density, redshift, and Doppler velocity in Inoue & Iwata (2008). We calculate the probability distribution of the IGM transmission in the F275W band for a random line of sight at $z = 2.518$ and find that $\exp(-\tau_{\rm IGM,800}) = 0.22^{+0.51}_{-0.22}$. By adopting $\exp(-\tau_{\rm IGM,800}) < 0.73$, we find that the absolute LyC escape fraction is $f_{\rm esc,abs} > 57\%$ and $f_{\rm esc,abs} > 28\%$ for the intrinsic $L_{1700}/L_{800} = 6$ and $L_{1700}/L_{800} = 3.5$, respectively.

3.3. Morphology of LyC

The A2218-Flanking A component is well detected in the F275W image. We find that the A2218-Flanking A in the F275W image elongates to the same direction of that in the F606W image. This similarity of the morphology in the F275W and F606W images indicates that the F275W flux is not from the foreground interlopers. Unfortunately, the F275W image is not deep enough to carry out a detailed morphology analysis for the diffuse part of the galaxy. With the high spatial resolution of the *HST* images, we study how the f_{1700}/f_{800} ratio changes across A2218-Flanking. We study a bright knot on the right (west) side of the A component (Figure 2), which is well detected in both F275W and F606W images. We measure the F275W and F606W flux density from the bright knot and find that $f_{800} = 0.0343 \pm 0.005\ \mu$Jy, $f_{1700} = 0.123 \pm 0.002\ \mu$Jy, which leads to $f_{1700}/f_{800} = 3.6 \pm 0.5$. This f_{1700}/f_{800} ratio is significantly lower than those found in the total of the lensed galaxy and A component, which suggests that the region with higher SFR surface density has a higher escape fraction.

4. Discussion

4.1. Properties of LyC Leaking Galaxies

It is essential to establish the relation between the LyC escape fraction and galaxy properties. This relation is crucial to predicting the LyC escape fraction of galaxies at the epoch of reionization, which cannot be directly measured (e.g., Faisst et al. 2016). Based on the confirmed LyC leaking galaxies at both low and high redshifts, studies try to connect the LyC escape fraction to varieties of galaxy properties, including dust extinction (reddening), interstellar absorption lines, Lyα emission lines, the flux ratios between [O III]$\lambda\lambda$4959, 5007 and [O II]λ3727, specific SFR (sSFR = SFR/M$_\star$), and SFR surface density (e.g., Heckman et al. 2011; Nakajima & Ouchi 2014; Izotov et al. 2016b; Reddy et al. 2016; Verhamme et al. 2017). Actually, the above galaxy properties are highly correlated. For example, Bian et al. (2016) found that the ionization parameter (i.e., [O III]$\lambda\lambda$4959, 5007/[O II]λ3727) increases significantly with increasing sSFRs and decreasing galaxy sizes in star-forming galaxies, and this trend may become stronger for high-redshift galaxies.

Therefore, it is crucial to understand the physical process behind these galaxy physical properties that regulates the LyC escape process in galaxies. Heckman et al. (2011) suggested that the extreme feedback caused by the high SFR surface density plays an important role in creating channels in the interstellar medium and enabling ionizing photons to escape from galaxies. Verhamme et al. (2017) did find a strong correlation between the LyC escape fraction and SFR surface density in low-redshift LyC emitters. This trend is consistent with our finding that a higher escape fraction is associated with the region with a higher SFR surface density in A2218-Flanking.

We compare the SFR surface density in A2218-Flanking with those in the other six lensed galaxies in this *HST* program. We find that the SFR surface densities are comparable in these seven galaxies ($\Sigma_{\rm SFR} \sim 1\ M_\odot\ {\rm yr}^{-1}\ {\rm kpc}^{-2}$). However, only A2218-Flanking has a high LyC escape fraction, and we do not detect significant LyC flux in the remaining six galaxies, suggesting that the LyC escape is less than 5%, assuming an average IGM optical depth for a given redshift. It is quite unlikely that the IGM transmission is an order of magnitude lower than average in all six galaxies. This piece of evidence suggests that, besides SFR surface density, there are also other properties regulating the LyC escape fraction. One unique property of A2218-Flanking is that it has an order of magnitude lower stellar mass compared to the remaining six galaxies (Bian et al. 2010; Richard et al. 2011). As suggested in the cosmological zoom-in simulations, the LyC escape fraction is higher in lower-mass dark matter halos (e.g., Kimm & Cen 2014), which presumably host galaxies with lower stellar mass.

It is worth noting that we cannot draw exclusive conclusions based on this small sample of galaxies because of the large systematic uncertainties of the $f1700/f800$ ratio and the unknown IGM optical depth for a random line of sight. Furthermore, the escape fraction may also depend on viewing angles, i.e., the ionizing radiation may be able to escape from galaxies only in some preferential directions (e.g., Cen & Kimm 2015). Therefore, a large sample ($\sim$100) of galaxies is required to study how the LyC escape fraction changes with galaxy properties.

5. Conclusion

In this Letter, we report a large LyC escape fraction (>57%) in a compact dwarf galaxy, A2218-Flanking. Our main results can be summarized as follows:

1. We carried out deep *HST*/WFC3 F275W UV imaging observations on A2218-Flanking. The F275W band covers the LyC emission at $\sim$800 Å.
2. We detect significant LyC emission from A2218-Flanking. From the flux density ratio between 1700 and 800 Å (f_{1700}/f_{800}), we find that the absolute LyC escape fraction is $f_{\rm abs,esc} > 0.57$.
3. We find that the region with a higher SFR surface density has a significantly lower f_{1700}/f_{800} ratio, suggesting a higher LyC escape in this region. This suggests that SFR surface density plays an important role in regulating the LyC escape fraction.
4. By comparing A2218-Flanking with other galaxies in this *HST* program without LyC flux detections, we find that the stellar masses of galaxies may also play roles in the LyC escaping process; the LyC escape is higher in galaxies with lower stellar mass.

We are grateful to the anonymous referee for a constructive report. We are thankful for the support for program #13349, provided by NASA through a grant from the Space Telescope Science Institute, which is operated by the Association of Universities for Research in Astronomy, Inc., under NASA contract NAS 5-26555.

Facility: HST/WFC3.

References

Bian, F., Fan, X., Bechtold, J., et al. 2010, ApJ, 725, 1877
Bian, F., Kewley, L. J., Dopita, M. A., & Juneau, S. 2016, ApJ, 822, 62
Bian, F., Stark, D. P., Fan, X., et al. 2015, ApJ, 806, 108
Bolzonella, M., Miralles, J.-M., & Pelló, R. 2000, A&A, 363, 476
Bouwens, R. J., Illingworth, G. D., Oesch, P. A., et al. 2015a, ApJ, 811, 140
Bouwens, R. J., Illingworth, G. D., Oesch, P. A., et al. 2015b, ApJ, 803, 34
Bouwens, R. J., Smit, R., Labbe, I., et al. 2016, ApJ, 831, 176
Bruzual, G., & Charlot, S. 2003, MNRAS, 344, 1000
Calzetti, D., Armus, L., Bohlin, R. C., et al. 2000, ApJ, 533, 682
Cen, R., & Kimm, T. 2015, ApJL, 801, L25
Cooke, J., Ryan-Weber, E. V., Garel, T., & Díaz, C. G. 2014, MNRAS, 441, 837
Faisst, A. L., Capak, P., Hsieh, B. C., et al. 2016, ApJ, 821, 122
Fan, X., Carilli, C. L., & Keating, B. 2006a, ARA&A, 44, 415
Fan, X., Strauss, M. A., Becker, R. H., et al. 2006b, AJ, 132, 117
Heckman, T. M., Borthakur, S., Overzier, R., et al. 2011, ApJ, 730, 5
Inoue, A. K., & Iwata, I. 2008, MNRAS, 387, 1681
Izotov, Y. I., Orlitová, I., Schaerer, D., et al. 2016a, Natur, 529, 178
Izotov, Y. I., Schaerer, D., Thuan, T. X., et al. 2016b, MNRAS, 461, 3683
Kimm, T., & Cen, R. 2014, ApJ, 788, 121
Leitet, E., Bergvall, N., Hayes, M., Linné, S., & Zackrisson, E. 2013, A&A, 553, A106
Leitherer, C., Hernandez, S., Lee, J. C., & Oey, M. S. 2016, ApJ, 823, 64
Livermore, R. C., Finkelstein, S. L., & Lotz, J. M. 2017, ApJ, 835, 113
Madau, P. 1995, ApJ, 441, 18
Naidu, R. P., Oesch, P. A., Reddy, N., et al. 2016, ApJ, submitted (arXiv:1611.07038)
Nakajima, K., & Ouchi, M. 2014, MNRAS, 442, 900
Nestor, D. B., Shapley, A. E., Kornei, K. A., Steidel, C. C., & Siana, B. 2013, ApJ, 765, 47
Nestor, D. B., Shapley, A. E., Steidel, C. C., & Siana, B. 2011, ApJ, 736, 18
Ouchi, M., Mobasher, B., Shimasaku, K., et al. 2009, ApJ, 706, 1136
Pawlik, A. H., Schaye, J., & van Scherpenzeel, E. 2009, MNRAS, 394, 1812
Pettini, M., & Pagel, B. E. J. 2004, MNRAS, 348, L59
Planck Collaboration, Adam, R., Aghanim, N., et al. 2016, A&A, 596, 108
Prevot, M. L., Lequeux, J., Prevot, L., Maurice, E., & Rocca-Volmerange, B. 1984, A&A, 132, 389
Reddy, N. A., Erb, D. K., Pettini, M., Steidel, C. C., & Shapley, A. E. 2010, ApJ, 712, 1070
Reddy, N. A., Steidel, C. C., Pettini, M., Bogosavljević, M., & Shapley, A. E. 2016, ApJ, 828, 108
Richard, J., Jones, T., Ellis, R., et al. 2011, MNRAS, 413, 643
Robertson, B. E., Furlanetto, S. R., Schneider, E., et al. 2013, ApJ, 768, 71
Rutkowski, M. J., Scarlata, C., Haardt, F., et al. 2016, ApJ, 819, 81
Salpeter, E. E. 1955, ApJ, 121, 161
Schenker, M. A., Ellis, R. S., Konidaris, N. P., & Stark, D. P. 2014, ApJ, 795, 20
Shapley, A. E., Steidel, C. C., Pettini, M., Adelberger, K. L., & Erb, D. K. 2006, ApJ, 651, 688
Shapley, A. E., Steidel, C. C., Strom, A. L., et al. 2016, ApJL, 826, L24
Siana, B., Shapley, A. E., Kulas, K. R., et al. 2015, ApJ, 804, 17
Siana, B., Teplitz, H. I., Colbert, J., et al. 2007, ApJ, 668, 62
Stark, D. P., Ellis, R. S., & Ouchi, M. 2011, ApJL, 728, L2
Steidel, C. C., Pettini, M., & Adelberger, K. L. 2001, ApJ, 546, 665
Vanzella, E., de Barros, S., Vasei, K., et al. 2016, ApJ, 825, 41
Vanzella, E., Giavalisco, M., Inoue, A. K., et al. 2010, ApJ, 725, 1011
Vanzella, E., Guo, Y., Giavalisco, M., et al. 2012, ApJ, 751, 70
Vasei, K., Siana, B., Shapley, A. E., et al. 2016, ApJ, 831, 38
Verhamme, A., Orlitova, I., Schaerer, D., et al. 2017, A&A, 597, 13